# Prelaunch Radiometric Calibration of the TanSat Atmospheric Carbon Dioxide Grating Spectrometer

Zhongdong Yang, Yuquan Zhen, Zenshan Yin, Chao Lin, Yanmeng Bi, Wu Liu, Qian Wang, Long Wang, Songyan Gu, and Longfei Tian

***Abstract*— TanSat is an important satellite in the Chinese Earth Observation Program which is designed to measure global atmospheric $CO_2$ concentrations from space. The first Chinese superhigh-resolution grating spectrometer for measuring atmospheric $CO_2$ is aboard TanSat. This spectrometer is a suite of three grating spectrometers that make coincident measurements of reflected sunlight in the near-infrared $CO_2$ band near 1.61 and 2.06 $\mu$m and in the molecular oxygen A-band ($O_2$A) at 0.76 $\mu$m. Their spectral resolving power ($\lambda/\Delta\lambda$) is $\sim$19 000, $\sim$12 800, and $\sim$12 250 in the $O_2$A, weak absorption band of molecular carbon dioxide band, and strong absorption of carbon dioxide band, respectively. This paper describes the laboratory radiometric calibration of the spectrometer suite, which consists of measurements of the dark current response, gain coefficients, and signal-to-noise ratio (SNR). The SNRs of each channel meet the mission requirements for the $O_2$A and weak $CO_2$ band but slightly miss the requirements in a few channels in the strong $CO_2$ band. The gain coefficients of the three bands have a negligible random error component and achieve very good stability. Most of the R-squared of gain coefficients model consist of five numbers of nine (e.g., 0.99999) after the decimal point, suggesting that the instrument has significant response linearity. The radiometric calibration results meet the requirements of an absolute calibration uncertainty of less than 5%.**

***Index Terms*— Atmospheric measurements, carbon dioxide, radiometric calibration, spectrometer.**

## I. Introduction

ATMOSPHERIC $CO_2$ is an important greenhouse gas in the climate system and plays a key role in climate change. Space-based remote sensing has received significant attention in recent years due to its potential to resolve many of the uncertainties in the spatial and temporal variability characterizing atmospheric $CO_2$ concentrations [1], [2]. However, obtaining the precise global atmospheric monthly $CO_2$ concentrations from space-based platforms at regional and global scales has proven to be challenging [3]–[7]. The radiometric calibration and characterization of spectrometers in the laboratory are essential in achieving the precise retrievals of atmospheric $CO_2$.

The Greenhouse Gases Observing Satellite (GOSAT) is a Japanese JAXA mission designed to monitor $CO_2$ and $CH_4$ globally using Fourier-transformed spectrometry of the thermal and near-infrared bands [8], [9]. GOSAT was launched on January 23, 2009, and has provided a large amount of global atmospheric $CO_2$ and $CH_4$ observational data. The Orbiting Carbon Observatory-2 (OCO-2), launched on July 2, 2014, is a NASA mission designed to measure the column-averaged $CO_2$ dry air mole fraction ($XCO_2$) [7]. The OCO-2 satellite carries a single instrument and incorporates three grating spectrometers that take coincident measurements of reflected sunlight in the near-infrared $CO_2$ band near 1.61 and 2.06 $\mu$m and in the molecular oxygen A-band ($O_2$A) at 0.76 $\mu$m. The three spectrometers have different characteristics and were calibrated independently [10], [11]. The OCO-2 has provided a large amount of observational data on atmospheric $CO_2$ since 2015 and may offer opportunities to study the global carbon cycle under climate change.

TanSat, the third satellite mission dedicated to measuring atmospheric $CO_2$ from space, can benefit from the lessons learned from the GOSAT and OCO-2 missions. "Tan" is the Chinese word for carbon, and TanSat means "carbon satellite." TanSat is a key satellite mission supported by the Ministry of Science and Technology of the China Earth Observation Program, and the mission is designed to measure global atmospheric $CO_2$ concentrations using a satellite in a Sun-synchronous, near-polar orbit. The measurement precision, accuracy, coverage, and resolution of the mission should meet the requirements of studying global climate change using modeling systems. TanSat is a one-satellite scientific exploratory mission. The satellite platform is actively stabilized over three axes, and its nominal design life is three years. TanSat is in a Sun-synchronous orbit with a local time of the descending node of $\sim$13 : 30 min, an orbital altitude of $\sim$700 km, and an

Manuscript received January 1, 2018; revised April 11, 2018; accepted April 18, 2018. Date of publication May 23, 2018; date of current version June 22, 2018. This work was supported by the National Satellite Meteorological Center, Changchun Institute of Optics, Fine Mechanics and Physics, and Shanghai Engineering Centre for Microsatellites through a major project of the Ministry of Science and Technology of the China Earth Observation Program (863), respectively, under Contract 2011AA12A104, Contract 201112A102, and Contract 201112A101. *(Corresponding author: Zhongdong Yang.)*

Z. Yang, Y. Bi, Q. Wang, and S. Gu are with the National Satellite Meteorological Center, China Meteorological Administration, Beijing 100081, China (e-mail: yangzd@cma.cn).

Y. Zhen, C. Lin, and L. Wang are with the Changchun Institute of Optics, Fine Mechanics and Physics, Chinese Academy of Sciences, Changchun 130033, China.

Z. Yin, W. Liu, and L. Tian are with the Shanghai Engineering Centre for Microsatellites, Chinese Academy of Sciences, Shanghai 201203, China.

Color versions of one or more of the figures in this paper are available online at http://ieeexplore.ieee.org.

Digital Object Identifier 10.1109/TGRS.2018.2829224

TABLE I
RADIOMETRIC PERFORMANCE REQUIREMENTS OF ACGS

| Band / Item | $O_2A$ | $WCO_2$ | $SCO_2$ |
|---|---|---|---|
| Dynamic Range (mW/m2/sr/nm ) | SNR=1@$3.2 \times 10^{-2}$ ~362.17 | SNR=1@$7.0 \times 10^{-3}$ ~60.50 | SNR=1@$5.8 \times 10^{-3}$ ~15.50 |
| SNR@($mW/m^2/sr/nm$ ) | 360@15.2 | 250@2.60 | 180@1.10 |
| Abs/Rel Calibration Error(%) | <5% / <3% | <5% / <3% | <5% / <3% |
| Calibration Nonlinearity Error (%) | <2% | <2% | <2% |
| Dark Current (DNs) Error | <5 DNs (after correction) | <5 DNs (after correction) | <5 DNs (after correction) |
| Radiance Response Uniformity (%) | >99.9% @ interior of band; >99% between bands. | >99.9% @ interior of band; >99% between bands. | >99.9% @ interior of band; >99% between bands. |

angle of inclination of 98.2°. TanSat was successfully launched on December 22, 2016. The National Satellite Meteorological Center of the China Meteorological Administration is in charge of TanSat data acquisition, processing, and dissemination. The main payload aboard TanSat is the atmospheric carbon dioxide grating spectrometer (ACGS), which measures three spectral bands: the oxygen-absorbing A-band, with a centroid wavelength of 760 nm, and the weak and strong carbon dioxide-absorbing bands, which are used to measure atmospheric $CO_2$ and have centroid wavelengths of 1610 and 2060 nm, respectively. The ACGS has a spatial resolution of $2 \times 3$ km, a swath of 20 km, a mass of 204 kg, and a peak power of 255 W.

This paper focuses on the laboratory radiometric calibration of the ACGS and is organized as follows. Section II gives a description of the instrument. Section III presents the laboratory radiometric calibration methodology, including the apparatus and methods used for testing, standard traceability, and the characterization of the essential parameters of the instrument. Section IV provides the results of this testing. The final section summarizes this paper and presents a review of the instrument characterization. The spectral calibration information for this instrument can be found in a companion paper.

## II. OVERVIEW OF THE TANSAT SPECTROMETER

The ACGS is an integrated suite of three grating spectrometers, one for each of the bands of interest. The ACGS was designed to measure solar radiation reflected by the earth-atmosphere system in three narrow bands at superhigh spectral, radiometric, and spatial resolutions. The $O_2A$, ranging from 758 to 778 nm, indicates the absorption of molecular oxygen, the weak absorption band of molecular carbon dioxide ($WCO_2$) ranges from 1594 to 1624 nm, and the strong absorption of carbon dioxide ($SCO_2$) band ranges from 2042 to 2082 nm.

### A. Radiometric Performance Requirements of the ACGS

The ACGS has critical radiometric, spectral, and spatial performance requirements. The radiometric performance requirements are summarized in Table I. In Table I, dynamic range refers to the range of spectral radiance energy values that can be measured in each band by the ACGS. This dynamic range of measurement is limited at one end of the range by the saturation of the detector. The other end of the dynamic range of measurement is limited by random noise or uncertainty in signal level, which are viewed as defining the sensitivity of the instrument in this paper. SNR denotes the signal-to-noise ratio, which is a measure that compares the level of a desired signal to the level of background noise. SNR is defined as the ratio of the signal power to the noise power and varies with the level of the signal. Calibration is a comparison of the values measured by the ACGS with those of a calibration standard of known accuracy, and the National Institute of Standards and Technology (NIST) standards are used in this paper. The absolute calibration error refers to the uncertainty compared with the NIST values, and the relative calibration error refers to the difference in the abs calibration between the three bands. Calibration nonlinearity error refers to the error due to the nonuniformity in the ACGS response from one end to the other end of the dynamic range. The dark current digital number (Dn) error refers to the uncertainty due to electrical noise and stray emissions. Radiance response uniformity refers to the calibration accuracy consistency in the spectral dimension of each band of the ACGS. This paper will describe how the ACGS instrument performed against the radiometric requirements.

### B. Basic Optical and Electric Configuration of the Instrument

The optical system of the ACGS consists of a telescope, collimator, reflectors, beam splitters, long slits, preoptical collimators, blazed diffraction gratings, and reimagers. Just before the photographs enter each spectrometer, a linear polarizer selects only the polarizing vector perpendicular to the entrance slit. A schematic of the ACGS is shown in Fig. 1. The spectrometers use three flat holographic gratings and operate at the first order.

At the focus of each spectrometer, one area array detector records the spectrum. This detector is similar to those in most common imaging spectrometers. One dimension is measured on a spatial field along the slit, and the spectrum is measured along another dimension perpendicular to the slit.

The $O_2A$ silicon detector has $320 \times 1242$ channels and operates at 268 K in the on-orbit environment. The two mercury–cadmium–telluride $CO_2$-band detectors have $240 \times 500$ channels and operate at 150 K, and the temperature is actively controlled to within ~0.3 K in orbit. The original $O_2A$ detector has an area of $22.5 \times 22.5$ $\mu$m and a spatial demension of 320 pixels, with the 17th original pixel to the 304th pixel being used to record radiation. Each set of 32 pixels is combined to yield one footprint, for a total of nine footprints in the spatial dimension, with a spectral dimension of 1242 pixels. Thus, the final number of $O_2A$ samples is nine footprints in

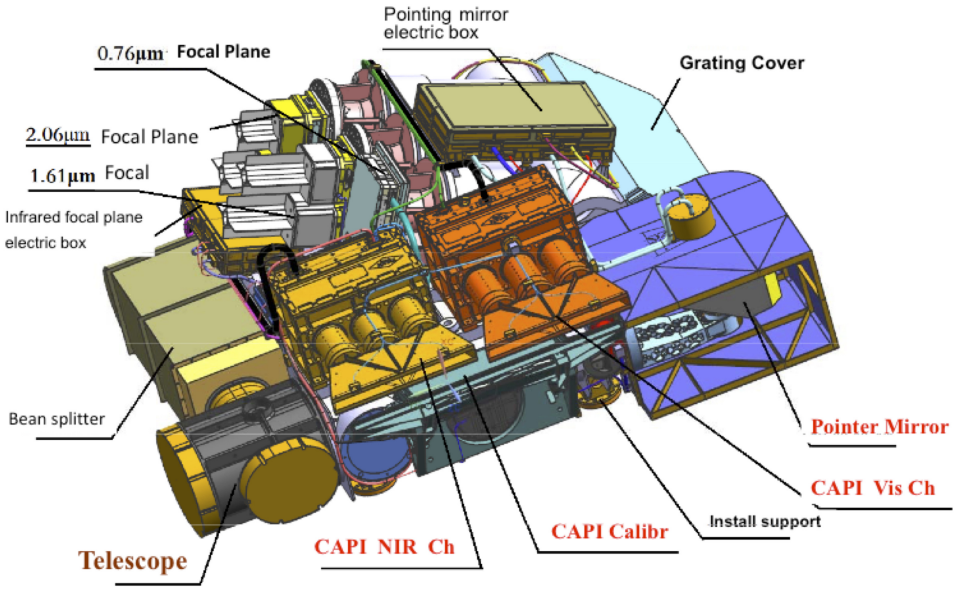


Fig. 1. Schematic of ACGS.

the spatial dimension $\times 1242$ pixels in the spectral dimension. The original detector of the two $CO_2$ bands has an area of $30 \times 30$ $\mu$m and a spatial dimension of 240 pixels, with the 13th original pixel to the 228th pixel being used to record radiation. Each set of 24 pixels is combined to yield one footprint, for a total of nine footprints in the spatial dimension. For the spectral dimension of 500 pixels, all the pixels are treated as spectral channels, and thus, the final number of samples in the $CO_2$ band is nine footprints in the spatial dimension $\times 500$ pixels in the spectral dimension. The detector of $O_2$A is a CCD55-30, from the e2v company; infrared focal pane arrays (FPAs) of $CO_2$ bands are NEPTUNE SW from Sofradir.

## III. Methodology

The ACGS was calibrated twice before it was assembled in the spacecraft bus in May 2016, and therefore, these testing data can be used to validate the stability of its characterizations. The first test was performed from September to November 2015, and the second test was performed from January to February 2016. The radiometric, spectral, polarization, and geometric features were characterized independently during the two calibration tests. All the characterization and calibration tests were conducted in a 3-m thermal vacuum chamber, simulating the on-orbit environment. Radiometric calibration was performed to measure the dark current offset, gain, linearity, and SNR for each detector in each band. This process is essential to achieving the retrieval precision required for atmospheric carbon dioxide concentration measurements. Similar works have been performed for the radiometric calibration of the GOSAT and OCO satellite instruments [8], [12]. These studies used a special transfer radiometer to read the spectral irradiance output in an integrating sphere to improve the precision of the calibration, but the special transfer radiometer did not work well; therefore, certain refinements to the photodiode transfer radiometer were carried out during the OCO-1 prelaunch radiometric calibration to correct calibration errors. There were many improvements in the OCO-2 prelaunch radiometric calibration [7], [11], [13], [14]. The integrating sphere and transfer radiometer were two key sets of testing equipment in this paper. An integrating sphere was used to standardize the irradiance source, and the transfer radiometer was used to translate the primary irradiance source, an NIST lamp standard, from the sphere to the ACGS.

### A. Testing Equipment

*1) Integrating Sphere:* In the laboratory radiometric calibration and characterization of the TanSat spectrometers, a 150-cm diameter integrating sphere with a 20-cm diameter exit port was used. The inner surface of the sphere was coated with barium sulfate. Two exterior 1000-W halogen tungsten lamps and one interior 600-W lamp were used as light sources in the sphere. One 5-mm Labsphere interior integrated silicon-unit detector, which was connected to one Labsphere electrostatic meter using the Bayonet Neill–Concelman interface, was used to monitor the stability of the sphere irradiance. There was a 25-level adjustable diaphragm between each exterior 1000-W halogen-tungsten lamp source and the entrance to the sphere. A cold water circulation machine was used to maintain a constant temperature at the position of the assembly lamps on the sphere. During the operational test, the sphere was continuously purged with high-purity nitrogen gas to eliminate the absorption gases $CO_2$, $O_2$, and $H_2O$. The sphere was powered by three Agilent N5770A constant-current sources, which can provide current stabilization for the halogen tungsten lamps with a precision of 3 mA; the uncertainty was less than 0.05%. The sphere fully illuminated the instrument entrance slit through a fused quartz window in the thermal vacuum chamber. However, two issues require

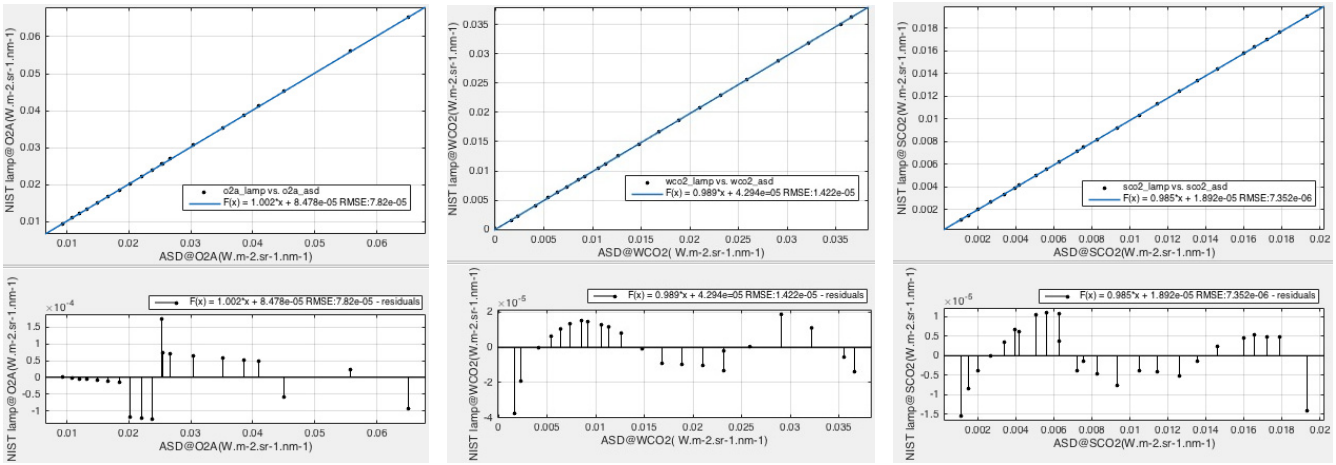


Fig. 2. Results of the statistical analysis of the ASD NIST standard traceability. (Left) $O_2A$. (Middle) $WCO_2$ band. (Right) $SCO_2$ band.

attention when using an integrating sphere in high-accuracy radiometric calibration testing. The first is irradiance stability, and the second is irradiance homogeneity at the exit port. The irradiance stability error of our integrating sphere as measured by the interior integrated silicon-unit detector was less than 0.3%. The irradiance homogeneity error of the exit port was 0.67% for the $O_2A$, 0.73% for the $WCO_2$ band, and 0.95% for the $SCO_2$ band using 37 spatial samplings uniformly distribution across the exit ports. The viewing angle irradiance homogeneity error for the center field of view was 0.46% for the $O_2A$, 0.37% for the $WCO_2$ band, and 0.29% for the $SCO_2$ band using 21 sampling angles in a 20° conical viewing field centered in the field of view of the exit port.

*2) Transfer Radiometer:* We need to know the intensity field of the integrating sphere to calibrate the radiometric characterization of the ACGS. A FieldSpec 4 Hi-Res analytical spectral device (ASD) was used to measure the spectral output of the integrating sphere as a transfer radiometer. The original calibration certificate of the FS4 HR 18251/1 ASD was traceable to NIST. We calibrated the ASD using a 1000-W quartz-halogen NIST lamp before the ACGS testing; the details will be given in Sectio III-A3.

*3) NIST Standard Traceability:* In this paper, a 1000-W quartz-halogen NIST lamp was used as the primary spectral irradiance standard. The spectral irradiance scale uncertainties ($k = 2$) of the lamp are 0.69% in the $O_2A$, 0.47% in the $WCO_2$ band, and 0.50% in the $SCO_2$. A Labsphere Spectralon diffuser was used for the spectral irradiance standard transfer from the lamp to the transfer radiometer with an apparatus. This apparatus was built to hold the lamp at 500 mm from the diffuser normal to the center of the diffuser and can accurately increase the distance between the lamp and the diffuser to change the magnitude of the irradiance from the lamp. The vendor provided the directional reflectance of the diffuser, which has the serial number 99AA01-0414-8942. The transfer radiometer viewed the diffuser at a fixed angle and position to obtain the irradiance value for the lamp with increasing distance between the lamp and the diffuser. This equipment, including the NIST lamp, Spectralon diffuser, and transfer radiometer, was shielded from stray ambient light. A high-precision, stabilized dc voltage source was used to ensure the stability of the lamp irradiance that illuminated the diffuser. The lamp illumination can be considered as a point source of light, and thus, the radiant flux density, also called irradiance, is linearly proportional to the solid angle [15]. The following equation is used to calculate the spectral irradiance of the diffuser with increasing distance between the lamp and the diffuser:

$$d\Omega(r, \lambda) = d\Omega_0(r_0, \lambda)\frac{r_0^2}{r^2} \tag{1}$$

where $r_0$ is the radius of the standard spheroid (here, 500 mm is used), $r$ is the radius of the spheroid, $\lambda$ is the wavelength of each band, $d\Omega(r, \lambda)$ is the spectral irradiance of the differential solid angle at the diffuse center of a spheroid, the center of which is normal to the diffuser center and the radius of which is $r$ mm, and $d\Omega_0(r_0, \lambda)$ is the spectral irradiance of the differential solid angle at the diffuse center of a spheroid, the center of which is normal to the diffuser center and the radius of which is 500 mm, as provided by the vendor.

We confirmed the precision and stability of the ASD FieldSpec 4 Hi-Res transfer radiometer by statistically analyzing the spectral irradiance calculated using (1) and the spectral irradiance readout of the ASD. The correlation of the statistical analysis of (1) and the ASD readout spectral irradiances was 99.8% [root-mean-square deviation (RMSE): 7.82e-05] for the $O_2A$, 98.9% (RMSE: 1.422e-05) for the $WCO_2$ band, and 98.5% (RMSE: 7.352e-06) for the $SCO_2$ band. Fig. 2 summarizes the statistical analysis of the spectral irradiances of the NIST lamp and the ASD transfer radiometer. The three graphs in the top present the correlations between the NIST lamp and the ASDs of the three bands, and the biases are presented in the bottom. All values are in units of ($W/m^2/sr/um$) or ($mW/m^2/sr/nm$). There is a very good agreement between the NIST lamp and the ASD: the bias was $0.2 \times 10^{-4}$ $mW/m^2/sr/nm$ for the $O_2A$, $1.1 \times 10^{-5}$ $mW/m^2/sr/nm$ for the WCO band, and $1.5 \times 10^{-5}$ $mW/m^2/sr/nm$ for the $SCO_2$ band.

The whole flowchart of the traceability and calibration of ACGS from the quartz-halogen NIST lamp, Labsphere

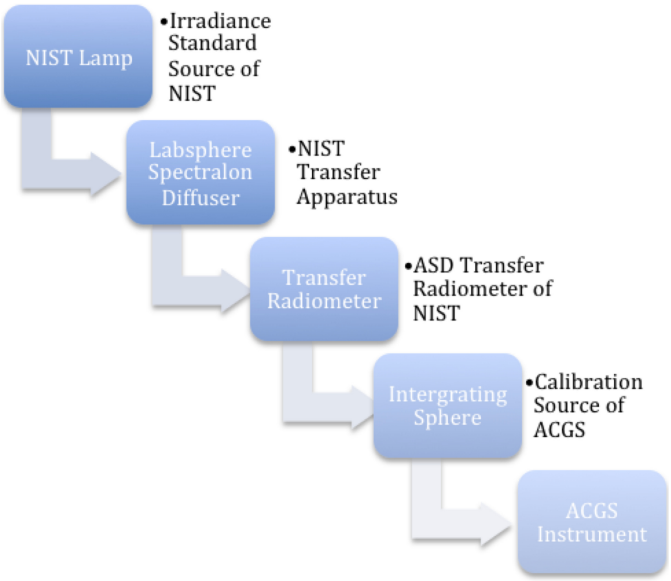


Fig. 3. Flowchart of standard traceability and calibration of ACGS.

Spectralon diffuser, ASD radiometer, and integrating sphere to calibrated ACGS can be seen in Fig. 3.

### *B. Testing and Data Processing Methods*

The method for testing the calibration and characterization configuration is shown in Fig. 4, which presents a schematic and all the equipment used in this paper. A total of 35 energy levels were set for the integrating sphere for the $O_2A$ from 1.1 to 407.8 mW/m$^2$/sr/nm, 34 energy levels from 0.5 to 66.0 mW/m$^2$/sr/nm for the $WCO_2$ band, and 31 energy levels from 0.1 to 19.1 mW/m$^2$/sr/nm for the $SCO_2$ band. The three bands of the ACGS were tested individually using the integrating sphere from high to low energy levels in observation mode, which has a 0.293-s frame sampling rate. Each energy level was maintained for 1.5 min to provide a sufficiently large sampling of the Dn values of each channel. The dark current was tested between energy levels using the irradiance shielding mode, and the irradiance intensity at the exit port was measured by the ASD simultaneously.

The dark current was also tested during temperature cycling testing of the ACGS before the calibration.

After comparing the results of the statistical analysis from the second- to sixth-order polynomial fittings, we found that the sixth-order polynomial coefficients are more stable. Thus, we choose the sixth-order least-squares polynomial fitting to compute the gain coefficients of the radiometric calibration for each channel in the three bands [see (2)] and evaluated the goodness of fit using the sum of squares due to error (SSE) and the R-squared. In principle, the radiometric calibration calculations belong to a category of statistics concerning large independent, representative samples. Thus, statistics can be useful in assessing the quality of the calibration

$$R = k \sum_{i=0}^{6} c_i (\mathrm{Dn} - \mathrm{Dn}_{\mathrm{dark}})^i \tag{2}$$

where $R$ is the radiant intensity of the entrance aperture of the ACGS as measured by the ASD, $c_i$ are the radiometric calibration gain coefficients for each channel with a sixth-order least-squares fitting, $k$ is the scaling parameter of the gain coefficients in flight, Dn is the digital number response in the observation model, and $\mathrm{Dn}_{\mathrm{dark}}$ is the digital number of the dark current response. In total, there are $9 \times 1242$ groups of gain coefficients in the radiometric calibration for the $O_2A$ and $9 \times 500$ for the $WCO_2$ and $SCO_2$ bands. Each group contains seven coefficients, from $c_0$ to $c_6$, that represent the response characteristics for each channel.

The calculation of the SNR of the ACGS is very similar to that performed for most optical remote sensing instruments. The SNR was characterized using the following equation at each energy level of the integrating sphere for each channel of the three bands:

$$\mathrm{SNR} = \frac{I_{\mathrm{mean}}}{\sqrt{\frac{1}{n-1}\sum_{i=1}^{n}(I_i - I_{\mathrm{mean}})^2}} \tag{3}$$

where SNR is the signal-to-noise ratio of one channel at a given energy level, $I_{\mathrm{mean}}$ is the average radiant intensity from $n$ samplings at a given energy level, $n$ is the number of samplings of radiant intensity at a given energy level, and $I_i$ is one sampling of radiant intensity at a given energy level.

## IV. Results

The main goal of this paper is to examine the radiometric characteristics of the ACGS through radiometric calibration testing in a laboratory setting. As mentioned in the introduction, the radiometric calibration accuracy and its stability are pivotal in realizing high-precision measurements of global atmospheric $CO_2$ concentrations [16]. In this section, we evaluate the radiometric calibration results, including the dark current response, gain coefficients, and SNR. Finally, we analyze the total error of the radiometric calibration and present on-orbit radiometric calibration results.

### *A. Dark Current*

Dark current is the response of a detector when it is not actively being irradiated. This measurement is the first key step of calibration. We measured the dark current response of the ACGS during thermal balance testing in the 3-m thermal vacuum chamber and evaluated the dark current temperature sensitivity simultaneously. The temperature during the thermal balance testing ranged from 258 K to 180 K.

The $O_2A$ dark current response is approximately 66 counts, and this result varies only between 2 and 3 counts between the high and low temperatures during thermal balance testing, indicating that this measure exhibits minimal temperature sensitivity. Because the temperature of the FPA is controlled to within 0.3 K on orbit, this sensitivity should be negligible. The dark current response in the $WCO_2$ band was found to be approximately 2850 counts, and there was a change of $\sim$100 counts in one simulated orbit during thermal balance testing. In contrast to that of the $O_2A$, the dark current response of the $WCO_2$ band was found to clearly depend on ambient temperature. Similarly, a significant sensitivity of the dark current response to ambient temperature was

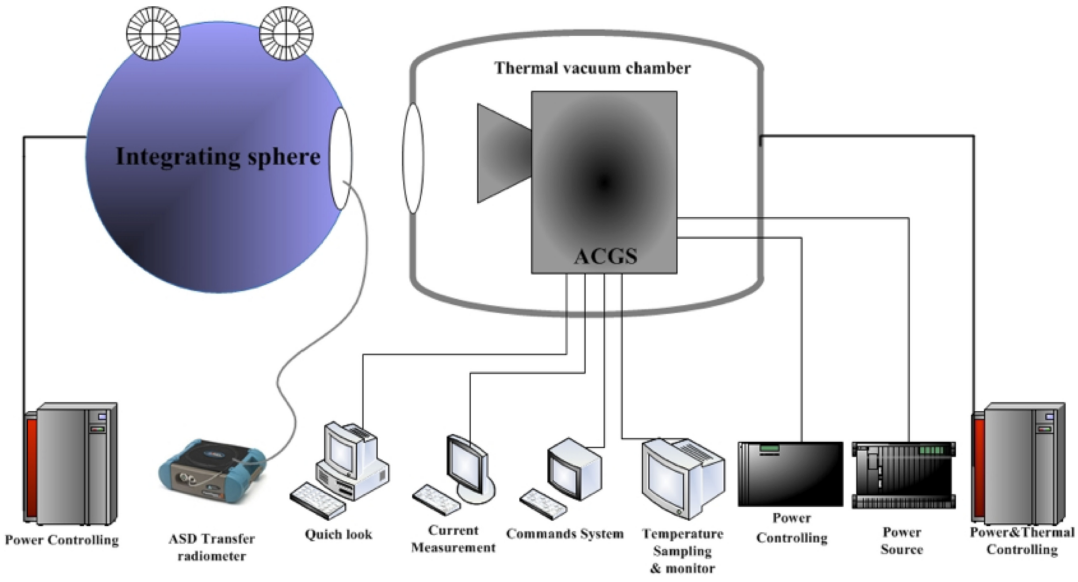


Fig. 4. Schematic of the ACGS radiometric calibration and characterization.

TABLE II
RADIOMETRIC CALIBRATION GAIN MODEL GOODNESS OF FIT

| Item / Band | SSE | | R-squared | |
|---|---|---|---|---|
| | Average | STD | Average | STD |
| $O_2$ A | $2.23 \times 10^{-6}$ | $1.50 \times 10^{-8}$ | 0.999991 | $6.45 \times 10^{-8}$ |
| $WCO_2$ | $3.47 \times 10^{-8}$ | $4.91 \times 10^{-10}$ | 0.999997 | $5.18 \times 10^{-8}$ |
| $SCO_2$ | $2.21 \times 10^{-9}$ | $8.23 \times 10^{-11}$ | 0.999998 | $1.54 \times 10^{-7}$ |

found for the $SCO_2$ band, the dark current response of which totaled to approximately 3000 counts during one simulated orbit. In addition, there was a change of ∼110 counts during the thermal balance testing. Thus, an ambient temperature sensitivity correction should be established for the dark current response for the two $CO_2$ bands.

The consistency of the dark current counts across the different channels in the three bands is very good, with a change in the Dn of a few. Most importantly, we found that the dark current patterns were very stable for each spectrometer between two tests.

The preliminary dark current responses as a function of temperature were established for the two $CO_2$ bands during the thermal vacuum tests (TVAC) testing, but these responses will be checked again when the platform is in orbit. In flight, the dark current responses of the three bands are measured twice during each orbit to monitor the stability of this measure in the operational mode. A full orbit on-board dark current response test of three bands is conducted during the first phase of orbital checkout, during which a few days of continuous measurements of dark current and FPA temperature are conducted simultaneously. Based on these testing data, we can construct more dark current response models to be used in the on-board calibration.

### *B. Gain Coefficients*

Gain coefficients provide us with knowledge of the response of the instrument to energy inputs. In general, the uniformity of the dynamic range, also called the linearity of response, and the stability of the gain coefficients are the key factors in quantitative remote sensing. Table II illustrates the statistical results of the goodness of fit obtained from the sixth-order least-squares polynomial fitting for calculating the radiometric calibration gain coefficients for each channel in the three bands. The SSEs of the three bands in Table II are very small in terms of both mean and standard deviation (STD) values, and the STDs are two orders of magnitude lower than the averages, indicating that this model fitting achieves a low random error. The R-squared values of the three bands in Table II are nearly 1.

In the statistical results of the goodness of fit, the standard deviations are very small, indicating that these model fits statistically account for most of the variation in the radiation response throughout the dynamic range.

The averages and standard deviations of the SSE and variance of the radiometric calibration gain demonstrated that the radiometric calibration fitting models for each band have a small random error components and account for most of the variation. Thus, these model fits should be made available for on-orbit radiometric calibration. We use the R-squared to evaluate the linearity of the instrument response. R-squared is a statistic that can give the information about the goodness of fit of our gain coefficient model. The R-squared of determination is a statistical measure of how well the regression line approximates the real data points. the R-squared of 1 indicates that the regression line perfectly fits the data. We found that

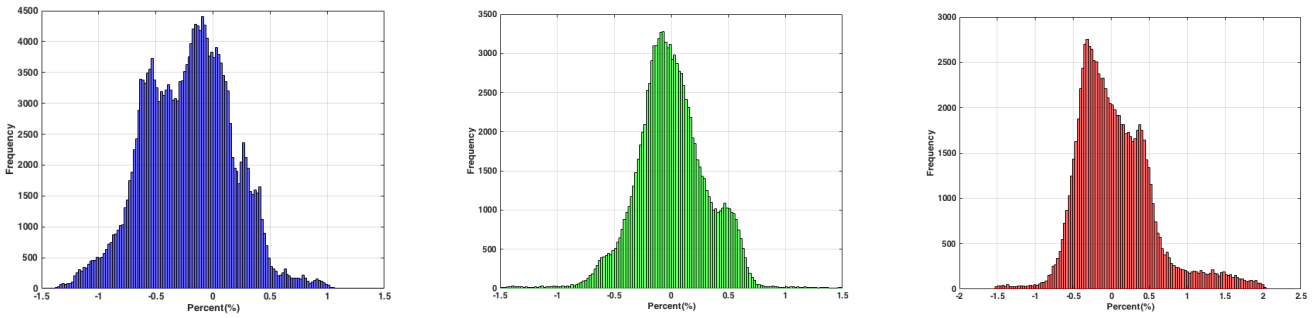


Fig. 5. Bias histograms between the two radiometric calibrations. (Left) $O_2$A. (Middle) $WCO_2$ band. (Right) $SCO_2$ band.

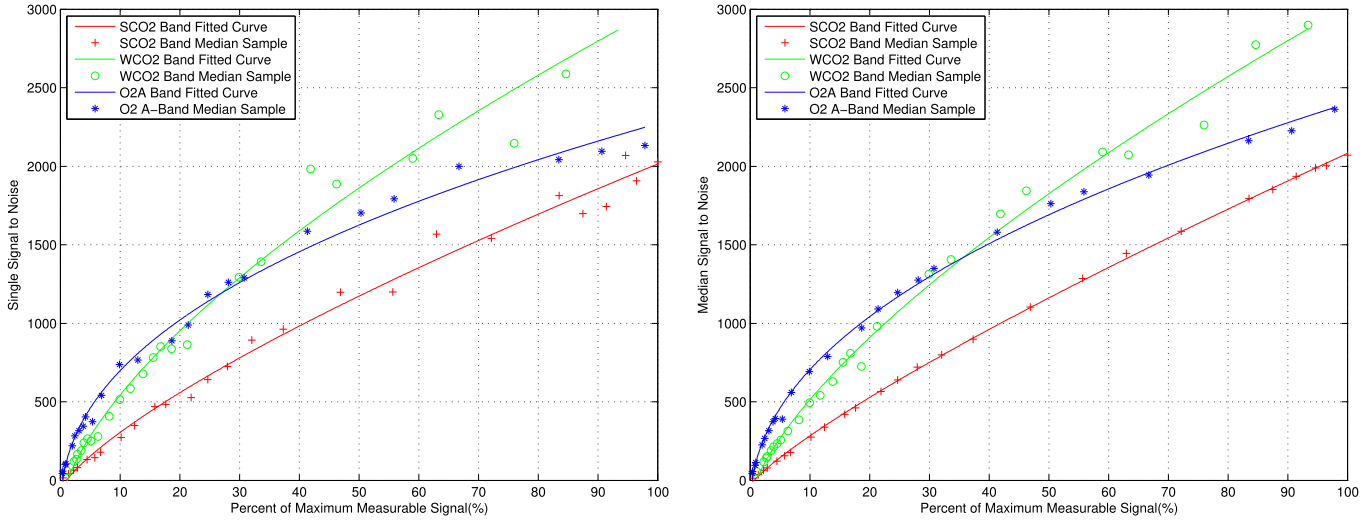


Fig. 6. ACGS SNR variation with the input intensity levels. (Left) Single channel near the center of the three bands. (Right) Median across all channels in each of the three bands.

most of the R-squared of gain coefficients model consist of five numbers of nine after decimal point. These results suggest that the ACGS exhibited significant response linearity during this radiometric calibration test.

The stability of the gain coefficients is very important for on-orbit data preprocessing and applications. The gain coefficients derived from the second radiometric calibration test will be used in orbit. We multiplied the gain coefficients acquired from the second test by the Dn of the first radiometric calibration, which was conducted in November 2015, to determine the radiance of the ACGS. We compared these results with those determined by the ASD during the first radiometric calibration test. Histograms of the bias between the ACGS and ASD results for the three bands are presented in Fig. 5. The bias between the two radiometric calibrations was very small, as shown in Fig. 5. The bias was less than 1.5% for the $O_2$A and $WCO_2$ band and ranged between $-1.55\%$ and $-2.1\%$ for the $SCO_2$ band. These results of the second calibration were clearly in good agreement with those of the first calibration, and the low bias validates the stability of the gain coefficients from the second radiometric calibration.

### C. Signal-to-Noise Ratio

The SNR is an essential parameter in the remote sensing estimation of atmospheric $CO_2$ concentrations. SNR is a measurement that compares the level of a desired signal to the level of background noise. SNR indicates how useful the data may be for a given measurement. The proper treatment of measurement noise is the dominant consideration in designing retrieval methods. All real measurements are subject to experimental error or noise, and therefore, any practical retrieval algorithm must allow for this [3]. Thus, we need to provide an accurate characterization of the ACGS SNR for the retrieval of the atmospheric $CO_2$ concentrations.

As an example, Fig. 6 illustrates the results of the laboratory-measured SNR for a single channel near the center of the FPA (left) and for the median (right) across all channels in each of the three bands at a variety of intensity levels taken during the second radiometric calibration. Fig. 6 also presents the resulting SNR model based on an exponential fit. As can be seen in Fig. 6, the mathematical relationship between SNR and intensity for a single channel approximated the exponential model. We checked all channels of the three bands, and a similar mathematical relation between the SNR and intensity was found in each. Thus, we used the exponential model in (4) to acquire the parameters C1, C2, and C3 of the SNR model for each channel using an optimal least-squares fitting. After obtaining these fit parameters for each channel of the three bands, the SNR could then be estimated for an arbitrary intensity $I$ using (4). This SNR in turn can be used to evaluate the on-board observational random error of the ACGS

$$\mathrm{SNR}(I) = C_1 \times I^{C_2} + C_3 \tag{4}$$

TABLE III
TOTAL ERROR ANALYSIS OF ACGS RADIOMETRIC CALIBRATION ($K = 1$)

| | $O_2A$ | $WCO_2$ | $SCO_2$ |
|---|---|---|---|
| NIST lamp uncertainty (%) | 0.70 | 0.50 | 0.50 |
| BRDF uncertainty of diffuser (%) | 1.49 | 1.88 | 1.88 |
| Distance measurement uncertainty (%) | 0.3 | 0.3 | 0.3 |
| Transfer radiometer uncertainty (%) | 2.0 | 2.0 | 2.0 |
| Stray light (empirical value) (%) | 1.0 | 1.0 | 1.0 |
| Sphere inner surface uniform (%) | 0.65 | 0.72 | 0.94 |
| Sphere exit angle luminance (%) | 0.5 | 0.5 | 0.5 |
| Sphere luminance stability (%) | 0.3 | 0.3 | 0.3 |
| Radiance response uncertainty of ACGS (%) | 2.0 | 2.0 | 2.0 |
| Total error/uncertainty (%) | 4.45 | 4.58 | 4.61 |

where SNR is the signal-to-noise ratio of one channel for a given intensity, $I$ is the intensity, and $C_1$, $C_2$, and $C_3$ are the parameters of the SNR model for each channel. The SNR values for each channel at the required intensity, which is 15.2 for the $O_2A$, 2.6 for the $WCO_2$, and 1.1 mW/m$^2$/sr/nm for the $SCO_2$ bands, meet the mission requirements for the $O_2A$ and weak $CO_2$ band but slightly miss the requirement in a few channels at longer wavelengths in the $SCO_2$ band.

### D. Total Error Analysis and On-Orbit Result

In this paper, the error has the same meaning as uncertainty, and we analyzed each stage of the error transfer from the NIST lamp to the ACGS instrument. We found that the total error of the radiometric calibration consists of the radiometric standard transfer, calibration source, and response of ACGS. The errors of the radiometric standard transfer consist of the uncertainty characterizing the NIST lamp, bidirectional reflectance distribution function of the diffuser, distance measurement between the lamp and the diffuser, transfer radiometer, and stray ambient light. The errors of the calibration source, the integrating sphere, consist of the uncertainty of the inner surface uniform, exit angle luminance uniformity, and luminance stability. The error of the ACGS response is the fitting calculation error of the gain coefficient. The details of the total error analysis result can be seen in Table III, where the radiometric calibration errors meet the 5% requirement in the three bands. We used the following equation to calculate the total error of the radiometric calibration:

$$\sigma_{\text{total}} = \sqrt{\sigma_1^2 + \sigma_2^2 + \sigma_3^2 + \sigma_4^2 + \sigma_5^2 + \cdots}. \tag{5}$$

## V. CONCLUSION

In this paper, we described the prelaunch radiometric calibration of the ACGS instrument aboard TanSat in terms of dark current response, gain coefficients, and SNR. As noted earlier, the radiometric calibration accuracy and its stability are pivotal to realizing high-precision retrievals of global atmospheric $CO_2$ concentrations. The TanSat was successfully launched on December 22, 2016, and these prelaunch calibration results have been used in the ground segment data preprocessing procedures.

The dark current response may also be called the zero shift in some works. Characterizing the dark current response is the first key step in the calibration of remote sensing instruments, especially with respect to the temperature sensitivity. The dark current response must be precisely deducted from the total response of each detector during calibration. We built preliminary models of the dark current response to temperature for the two $CO_2$ bands during the TVAC testing. More precise dark current response models must be built during the on-board check out and will be used in the on-board calibration.

The SNR of the ACGS meets the mission requirements for each channel of the $O_2A$ and the weak $CO_2$ band but slightly misses the requirements in a few channels in the strong $CO_2$ band. This issue impacts the retrieval accuracy of the $XCO_2$ under certain weather and surface conditions. Future work on new $CO_2$ instruments should focus on cooling and temperature control to create lower ambient temperatures for the detector, which should improve the SNR of the instrument. Exponential SNR models were built during this calibration, and these models could be used to estimate the random error of the on-board measurements of the ACGS and, also, could be used in retrieval algorithm of $XCO_2$.

The gain coefficient models for the three bands of the ACGS have very small error components, and these models accounted for most of the variance and are very stable. Thus, these gain coefficients should be made available for on-orbit radiometric calibration. Most of the R-squared of gain coefficients model consist of five numbers of nine after decimal point, suggesting that the ACGS has significant response linearity. These results show that the radiometric calibration errors are smaller than the required absolute calibration uncertainty of 5%.

## ACKNOWLEDGMENT

The authors would like to thank all the Changchun Institute of Optics, Fine Mechanics and Physics employees who worked wisely and tirelessly to obtain the atmospheric carbon dioxide grating spectrometer TVAC data. The authors would also like to thank the two anonymous reviewers for their thoughtful comments on the original manuscript. Z. Yang is a Senior Scientist with National Satellite Meteorological Center, and also a Chief Scientist of both the TanSat ground segment and the ground segment of the FengYun-3 satellites and takes a leading role in the data processing and algorithm development of products for the FengYun-3 meteorological satellites and TanSat.

## REFERENCES

[1] F. Chevallier, "Impact of correlated observation errors on inverted $CO_2$ surface fluxes from OCO measurements," *Geophys. Res. Lett.*, vol. 34, L24804, 2007, doi: 10.1029/2007GL030463.
[2] D. Crisp *et al.*, "The Orbiting Carbon Observatory (OCO) mission," *Adv. Space Res.*, vol. 34, no. 4, pp. 700–709, 2004.
[3] C. D. Rodgers, *Inverse Methods For Atmospheric Sounding: Theory and Practice*. Singapore: World Scientific, 2000.
[4] C. E. D. Miller, "Precision requirements for space-based $X_{CO_2}$ data," *J. Geophys. Res. Atmos.*, vol. 112, no. 10, pp. 1–19, 2007.
[5] B. J. Connor, H. Boesch, G. Toon, B. Sen, C. Miller, and D. Crisp, "Orbiting carbon observatory: Inverse method and prospective error analysis," *J. Geophys. Res.*, vol. 113, D05305, 2008, doi: 10.1029/2006JD008336.
[6] S. Boland, L. Brown, P. Ciais, B. Connor, W. Hole, and I. Fung, "The need for atmospheric carbon dioxide measurements from space: Contributions from a rapid reflight of the Orbiting Carbon Observatory," *Earth Sci.*, pp. 1–38, May 2009.

[7] D. Crisp *et al.*, "The on-orbit performance of the Orbiting Carbon Observatory-2 (OCO-2) instrument and its radiometrically calibrated products," *Atmos. Meas. Techn. Discuss.*, vol. 10, no. 1, pp. 59–81, 2017. [Online]. Available: http://www.atmos-meas-tech-discuss.net/amt-2016-281
[8] F. Sakuma *et al.*, "OCO/GOSAT preflight cross-calibration experiment," *IEEE Trans. Geosci. Remote Sens.*, vol. 48, no. 1, pp. 585–599, Jan. 2010.
[9] C. Frankenberg *et al.*, "The Orbiting Carbon Observatory (OCO-2): Spectrometer performance evaluation using pre-launch direct sun measurements," *Atmos. Meas. Techn.*, vol. 8, no. 1, pp. 301–313, 2015.
[10] R. Pollock *et al.*, "The Orbiting Carbon Observatory instrument: Performance of the OCO instrument and plans for the OCO-2 instrument," *Proc. SPIE*, vol. 7826, p. 78260W, Oct. 2010.
[11] R. Rosenberg, S. Maxwell, B. C. Johnson, L. Chapsky, R. A. M. Lee, and R. Pollock, "Preflight radiometric calibration of Orbiting Carbon Observatory 2," *IEEE Trans. Geosci. Remote Sens.*, vol. 55, no. 4, pp. 1994–2006, Apr. 2017. [Online]. Available: http://ieeexplore.ieee.org/document/7809060
[12] C. E. Miller, L. R. Brown, R. A. Toth, D. C. Benner, and V. M. Devi, "Spectroscopic challenges for high accuracy retrievals of atmospheric $CO_2$ and the Orbiting Carbon Observatory (OCO) experiment," *Comptes Rendus Physique*, vol. 6, no. 8, pp. 876–887, 2005.
[13] C. W. O'Dell *et al.*, "Preflight radiometric calibration of the Orbiting Carbon Observatory," *IEEE Trans. Geosci. Remote Sens.*, vol. 49, no. 6, pp. 2438–2447, Jun. 2011. [Online]. Available: http://ieeexplore.ieee.org/lpdocs/epic03/wrapper.htm?arnumber=5673019
[14] A. Eldering *et al.*, "The Orbiting Carbon Observatory-2: First 18 months of science data products," *Atmos. Meas. Techn.*, vol. 10, no. 2, pp. 549–563, 2017.
[15] K. N. Liou, *An Introduction to Atmospheric Radiation* (International Geophysics), vol. 84, 2nd ed. New York, NY, USA: Academic, Apr. 2002.
[16] B. Connor *et al.*, "Quantification of uncertainties in OCO-2 measurements of $XCO_2$: Simulations and linear error analysis," *Atmos. Meas. Techn.*, vol. 9, no. 10, pp. 5227–5238, 2016.

**Zhongdong Yang** received the B.S. and M.S. degrees from Xinjiang University, Xinjiang, China, in 1987 and 1990, respectively, and the Ph.D. degree in remote sensing science from the Institute of Geology, Beijing, China, in 1997.

From 2010, he was the Chief Scientist with the Ground Segment Project of FY-3 meteorological satellite series. He is currently a Senior Scientist with the National Satellite Meteorological Center, Chinese Meteorological Administration, Beijing. He is also the Chief Scientist of TanSat ground segment and takes a leading role in data processing, algorithm developments, and the ground segment of FY-3 Satellites and TanSat.

**Yuquan Zhen** received the Ph.D. degree in optical science from the Changchun Institute of Optics, Fine Mechanics and Physics, Chinese Academy of Sciences, Changchun, China, in 1999.

He was a Deputy Project Scientist for the Chinese Carbon Dioxide Observation Satellite (TanSat) Mission with the with the Changchun Institute of Optics, Fine Mechanics and Physics, where he is currently a Senior Research Scientist and the Director of Space Optics Department, and serving as the Project Manager for the Carbon Dioxide Spectrometer.

**Zenshan Yin** received the Ph.D. degree from Zhejiang University, Hangzhou, China.

He is currently a Professor and the Chief Designer of Global Carbon Dioxide Monitoring Scientific Experimental Satellite (TanSat). He is also with the Shanghai Engineering Centre for Microsatellites, Chinese Academy of Sciences, Shanghai, China. He has been selected as an expert of the National High Technology Research and Development Program of China and chosen by the National High-Level Personnel of Special Support Program. His research interests include satellite system design.

**Chao Lin** received the M.S. degree in mechanical engineering from Jilin University, Changchun, China, in 2009.

He was a Deputy Project Lead for the Carbon Dioxide Spectrometer and mainly in charge of spectral and radiometric calibration of the Carbon Dioxide Spectrometer with the Changchun Institute of Optics, Fine Mechanics and Physics, Changchun, where he is currently an Assistant Scientist with the Space Optics Department.

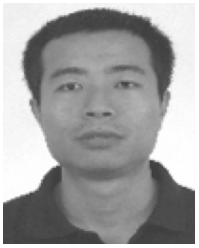

**Yanmeng Bi** received the Ph.D. degree in atmospheric physics science from Peking University, Beijing, China.

He is currently a member of the TanSat Team with the National Satellite Meteorological Center, Beijing, China, where he is responsible for the preprocessing of TanSat data. His research interests include remote sensing of $CO_2$ from satellite.

**Wu Liu** received the M.S. degree from Beihang University, Beijing, China.

He is currently a Designer of the Global Carbon Dioxide Monitoring Scientific Experimental Satellite (TanSat). He is also with the Shanghai Engineering Centre for Microsatellites, Chinese Academy of Sciences, Shanghai, China. His research interests include satellite system design.

**Qian Wang** received the M.S. degree from the Chinese Academy of Meteorological Sciences, Beijing, China, in 2014.

She is currently a member of the TanSat Team with the National Satellite Meteorological Center, Beijing. Her research interests include remote sensing of atmospheric composition from satellite.

**Long Wang** received the M.S. degree in mechanical engineering from Jilin University, Changchun, China, in 2011.

He is currently an Assistant Scientist with the Space Optics Department, Changchun Institute of Optics, Fine Mechanics and Physics, Changchun. He is also an Instrument Architect with the Carbon Dioxide Spectrometer and mainly in charge of Pointing Mirror Unit.

**Songyan Gu** received the Ph.D. degree from Peking University, Beijing, China.

She is currently the Deputy Chief Designer of the FY-3 Satellite. He is also a member of the TanSat Team with the National Satellite Meteorological Center, Beijing. She is responsible for the preprocessing of TanSat data.

**Longfei Tian** received the M.S. degree from Northwestern Polytechnical University, Fremont, CA, USA.

He is currently a Designer of the Global Carbon Dioxide Monitoring Scientific Experimental Satellite (TanSat). He is also with the Shanghai Engineering Centre for Microsatellites, Chinese Academy of Sciences, Shanghai, China. His research interests include satellite system design.